Double-resonance spectroscopy of transitions between autoionizing levels of atomic oxygen

S. T. Pratt, P. M. Dehmer, and J. L. Dehmer
Argonne National Laboratory, Argonne, Illinois 60439
(Received 26 November 1990)

Double-resonance spectroscopy is used to study transitions between autoionizing levels of atomic oxygen. The first laser is used to produce oxygen atoms in the $1s^2 2s^2 2p^4\,{}^1D_2$ level by photodissociation of N_2O and to excite two-photon transitions from the ${}^1D_2$ level to the long-lived $({}^2D^\circ)3p\,{}^1F_3$ autoionizing level. The second laser is used to probe transitions from the ${}^1F_3$ level to higher-energy autoionizing levels as well as to the $O^+\,{}^2D^\circ$ direct-ionization continuum. The transitions are detected by using a magnetic bottle electron spectrometer to monitor photoelectrons selectively with the kinetic energy specific to the process of interest. New transitions to the $({}^2D^\circ_{5/2,3/2})ns'$ and nd' Rydberg-series members with $n=16-31$ are observed. The intensity dependence of these results has also been studied, and the implications of this relatively low-power measurement for above-threshold ionization are discussed.

I. INTRODUCTION

Although optical transitions between autoionizing levels of atoms are important for the detailed understanding of diverse phenomena such as electron-ion recombination and above-threshold ionization (ATI),[1–5] explicit experimental evidence for these transitions is quite scarce.[6–8] To observe transitions between autoionizing levels, the photoabsorption rate must be high enough to compete with the autoionization rate of the lower level of the transition. Unfortunately, autoionization is usually quite rapid, requiring high laser intensities that tend to saturate and broaden any resonant structure arising from transitions between autoionizing levels. Thus, while the observation of ATI (that is, the absorption of more photons than are energetically necessary to ionize an atom with the additional energy deposited into the kinetic energy of the ejected electron) is clear evidence for transitions within the ionization continuum, there is little evidence for a wavelength dependence of the ATI signal that would reflect the resonant structure of transitions between autoionizing levels.

Rather than increase the photoabsorption rate to compete with the autoionization rate, one approach to the study of transitions between autoionizing levels is to choose a system in which the autoionization rate of the lower level of the transition is small. Transitions from metastable states in the ionization continuum have been observed in several earlier experiments.[6,7] For example, Spong *et al.*[6] have used laser-depletion spectroscopy to study transitions from a metastable, doubly excited level of rubidium to higher-energy autoionizing levels and to determine the lifetimes of these levels. Although the metastable level is energetically above the $Rb^+\ {}^2S_0$ ground state, autoionization is strongly spin forbidden. Thus fluorescence is the dominant decay path for the metastable level, and transitions to higher-energy levels were detected by the depletion of this fluorescence. Van Woerkum, Story, and Cooke[7] have observed a transition from a metastable autoionizing level of Ba to a higher-energy, short-lived autoionizing level by using a retarding field to selectively detect the fast photoelectrons produced by autoionization of the upper level and to discriminate against the slow photoelectrons produced by autoionization of the metastable level. This signal was monitored as the time delay between the laser pulse populating the metastable level and the laser pulse driving the probe transition was varied to determine the lifetime (190 nsec) of the metastable level. Finally, in a related study, Gallagher *et al.*[8] have demonstrated two-photon excitation of an autoionizating level of Ba by tuning the first laser to a minimum in the one-photon ionization cross section that was very near a maximum in the cross section, and by tuning the second laser to the energy of the transition from the minimum to a higher-energy autoionizing level. In this way the two-photon amplitude was large due to the nearly resonant one-photon transition, but ionization by the first laser alone was negligible due to the small cross section.

We have recently studied the photoionization dynamics of the $({}^2D^\circ)3p\,{}^1P_1$ and ${}^1F_3$ autoionizing levels of atomic oxygen.[9] A schematic diagram of the relevant energy levels is shown in Fig. 1.[10–12] Atomic oxygen was produced in the $1s^2 2s^2 2p^4\,{}^1D_2$ level by photodissociation of a suitable precursor[13] and excited to the $({}^2D^\circ)3p\,{}^1P_1$ and ${}^1F_3$ levels by two-photon absorption. Although these levels lie above the $O^+\,{}^4S^\circ_{3/2}$ ionization threshold, they are forbidden to autoionize within the approximations of *LS* coupling and can only decay by spin-orbit or spin-spin interactions. Although the lifetimes of these levels ($\sim 3\times 10^{-11}$ and $\sim 6\times 10^{-10}$ sec for ${}^1P_1$ and ${}^1F_3$, respectively)[9,12] are significantly shorter than those of the metastable levels discussed above, they are long enough to permit competitive photoionization from the ${}^1P_1$ and ${}^1F_3$ levels into the ${}^2D^\circ$ continuum at relatively low laser intensities, thus providing a convenient system in which to study phenomena such as transitions between autoionizing levels and above-threshold ionization. Indeed, by us-

 ©1991 The American Physical Society

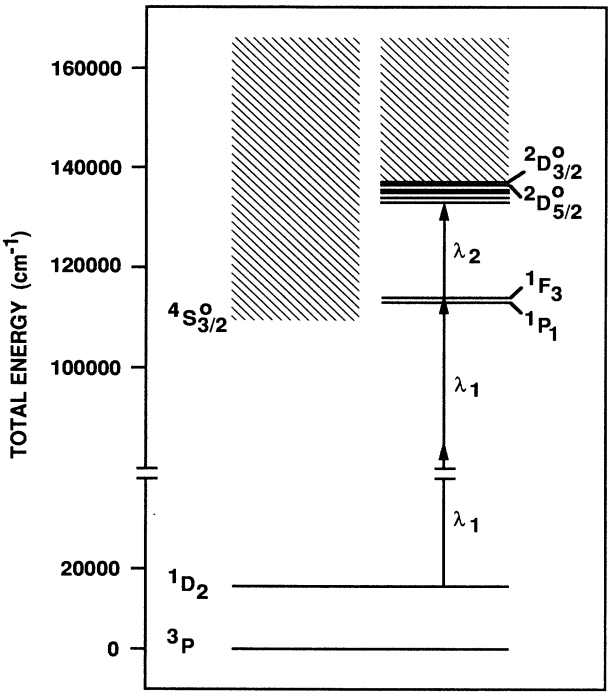

FIG. 1. Schematic energy-level diagram of the atomic oxygen levels of interest.

ing photoelectron spectroscopy we have demonstrated[9] that at low laser intensities ($\sim 3\times 10^9$ W/cm^2) photoionization from the $^1F_3$ level into the $^2D^\circ$ continuum competes effectively with autoionization.

In this paper we present the results of new double-resonance studies of transitions between autoionizing levels of atomic oxygen. As in our earlier study,[9] the $^1F_3$level is populated by two-photon excitation from the $^1D_2$ level, but now a second tunable laser is used to probe transitions from the $^1F_3$ level to higher-lying autoionizing levels as well as to the $^2D^\circ$ ionization continuum. The addition of the second laser does not produce a significant increase in the O^+ ion signal because the $^1F_3$ level also produces O^+ ions directly by autoionization. For this reason, we have used electron spectrometry to monitor the photoelectrons produced with the kinetic energy specific to the two-color process of interest. This allows the direct observation of transitions between autoionizing levels and of the wavelength dependence of the above-threshold ionization signal. In addition, we have observed new transitions from the $^1F_3$ level to the $(^2D^\circ_{5/2,3/2})ns'$ and nd' Rydberg series with principal quantum numbers in $n=16-34$. To our knowledge, the only previous double-resonance study of atomic oxygen was performed by Kröll *et al.*[14] and focused on transitions within the triplet manifold well below the $^4S^\circ_{3/2}$ ionization threshold.

II. EXPERIMENT

The experiments were performed by using two Nd:YAG pumped dye lasers (where YAG is yttrium aluminum garnet) and a magnetic bottle electron spectrometer that has been described previously.[15,16] In our earlier study of atomic oxygen,[9] the pump laser light at 203.8 nm was generated by frequency tripling the output of a dye laser operating at 611.4 nm. In the present study, 203.8-nm light was generated by mixing the 354.7-nm third-harmonic light from the Nd:YAG laser with the 479.1-nm fundamental light from the dye laser in a β-barium borate crystal. Owing to the large linewidth of the 354.7-nm beam, the linewidth of the light generated by mixing (~ 1 cm^{-1}) is considerably larger than that generated by frequency tripling (~ 0.2 cm^{-1}); however, this has no impact on the results of the present experiments. In addition, the mixing technique is simpler than the tripling scheme and requires considerably less equipment. The second Nd:YAG pumped dye laser was used to generate probe light between 455 and 435 nm. The counterpropagating pump and probe laser beams were focused into the ionization region of the magnetic bottle electron spectrometer by using 200- and 250-mm focal length lenses, respectively. The pump laser pulse energies were typically 10–30 μJ, and the probe laser pulse energies were varied from 50 to 100 μJ. The two lasers were synchronized by a series of digital delay generators so that the pulses were temporally overlapped in the ionization region of the electron spectrometer.

The details of the magnetic bottle spectrometer and the conversion of the time-of-flight spectra into energy spectra have been discussed previously.[15,16] In the present experiments, the electron spectrometer was used in two different modes. In the first mode, the wavelengths of the lasers were tuned to the features of interest and then held constant as the photoelectron spectrum was recorded by using a transient digitizer to capture the complete time-of-flight spectrum on each laser shot. Spectra were then averaged over 5000–10 000 laser shots to achieve a good signal-to-noise ratio. In the second (or constant ionic state) mode, the gate of a charge-sensitive analog-to-digitial converter was set to accept only those photoelectrons with the kinetic energy corresponding to the excitation process of interest, and the probe laser was then scanned to map out the wavelength dependence of this process. The wavelength of the probe laser was calibrated by using a commercial Fizeau wavementer, which was in turn calibrated by using the optogalvanic effect in neon and uranium.[17] The calibration of the probe laser wavelength is good to ± 0.3 cm^{-1}.

As discussed previously,[9] photodissociation of N_2O at 203.8 nm may produce $O\,^1D_2$ atoms with a significant amount of translational energy. This energy would produce a Doppler broadening of the observed $^1F_3 \leftarrow {}^1D_2$ two-photon transition and obscure its natural linewidth. In our earlier study with a narrow-band source of 203.8-nm light, the measured linewidth was ~ 0.8 cm^{-1}, corresponding to a "lifetime" of 4.3×10^{-11} sec. This is much shorter than the $\sim 6\times 10^{-10}$ sec lifetime that we have estimated from the photoelectron spectrum,[9] and indicates that the transition is significantly Doppler broadened. In the double resonance spectra discussed below, the probe laser must pump the atoms from the $^1F_3$ level in competition with the natural decay of the level by autoionization

and fluorescence. As the probe transition rate is increased to the point where it effectively competes with the natural decay of the $^1F_3$ level, the lifetime is decreased, and the linewidth of the pump transition will increase. However, with the present resolution and Doppler broadening, no increase in the linewidth of the $^1F_3 \leftarrow {}^1D_2$ transition has been observed.

III. GENERAL BACKGROUND

In this section we review the characteristics of the $(^2D^\circ)3p\ ^1P_1$ and $^1F_3$ levels and discuss the transitions expected from the $^1F_3$ level to higher-lying excited states. The singlet levels of atomic oxygen in the energy region between the $O^+\ ^4S^\circ_{3/2}$ ground state and the $^2D^\circ$ excited state are forbidden to autoionize within the approximations of LS coupling because coupling the $O^+\ ^4S^\circ_{3/2}$ ionic state with an electron can produce only triplet and quintet continua. For the same reason, direct two-photon (and single-photon) ionization from the $^1D_2$ level is also forbidden in this energy region. In fact, the first identification of the $^1P_1$ and $^1F_3$ levels came from the emission studies of Edlén[11] and Eriksson and Isberg,[12] who observed transitions from both the $^1P_1$ and $^1F_3$ levels to lower energy levels and from higher energy levels to the $^1P_1$ and $^1F_3$ levels. Transitions involving the $^1P_1$ level were significantly broadened and weaker than expected,[12] indicating that autoionization was strongly competing with fluorescence in this case. Although no broadening of the $^1F_3$ level was observed in the emission studies, we have recently shown that both the $(^2D^\circ)3p\ ^1P_1$ and $^1F_3$ levels have significant branching ratios for autoionization.[9] From a measurement of the linewidth of the $^1P_1$ transitions, Eriksson and Isberg[12] determined the lifetime of the $^1P_1$ level to be 3×10^{-11} sec. Although they gave no value for the $^1F_3$ lifetime, by using the results from our photoelectron study we have estimated this lifetime to be $\sim 6\times10^{-10}$ sec.[9] The shorter lifetime of the $^1P_1$ level is consistent with the selection rules for autoionization, which show that the $^1P_1$ level can autoionize by spin-orbit or spin-spin interactions, while the $^1F_3$ level can only autoionize by spin-spin interactions.[18,19]

The allowed transitions from the $(^2D^\circ)np\ ^1F_3$ level are now discussed. The $O^+\ ^4S^\circ_{3/2}$ and $^2D^\circ_{5/2,3/2}$ levels shown in Fig. 1 and the $O^+\ ^2P^\circ$ levels ($^2P^\circ_{3/2}$ at 150 303.6 and $^2P^\circ_{1/2}$ at 150 305.1 cm^{-1}) are all based on the $1s^22s^22p^3$ configuration, and electric dipole transitions between them are forbidden.[20] In addition, the first electronically excited configuration of O^+ corresponds to $1s^22s2p^4$ and produces three levels about 120 000 cm^{-1} above the $^4S^\circ_{3/2}$ ground state.[10] Thus, in the wavelength region of the present study, core-switching transitions from the $(^2D^\circ)3p\ ^1F_3$ level are either symmetry forbidden or energetically forbidden, and therefore the only expected transitions involve excitation of the $3p$ Rydberg electron. In what follows, quantum numbers for the $^1D_2$ initial state will be labeled with double primes (i.e., $J''=2$), quantum numbers for the $^1F_3$ level will be labeled with single primes ($J'=3$), and quantum numbers for the upper level of the probe transition will have no primes ($J=2$, 3, or 4).

The $(^2D^\circ)3p$ configuration is a very good approximation to the $^1F_3$ level, and the nearest $(^2D^\circ)nf$ level is at almost 16 000 cm^{-1} higher in energy.[10] Thus the expected transitions from the $^1F_3$ level are to $(^2D^\circ)ns'$ and nd' Rydberg series with $J=2$, 3, and 4. Some of the $(^2D^\circ)ns'$ and nd' states with $J=1$, 2, and 3 have been observed previously by Huffman, Larrabee, and Tanaka[21] in single-photon absorption studies from the $1s^22s^22p^4\ ^1D_2$ and $^1S_0$ levels. However, those studies were limited to $(^2D^\circ)ns'$ and nd' Rydberg series with principal quantum numbers $n \leq 14$. In the present experiment it is possible to extend these series to much higher principal quantum numbers.

The $O^+\ ^2D^\circ$ level is split into two spin-orbit components with the $^2D^\circ_{5/2}$ level 19.79 cm^{-1} lower in energy than the $^2D^\circ_{3/2}$ level.[10] Although Huffman, Larrabee, and Tanaka[21,22] labeled their observed Rydberg series by using LS coupling, for medium to high principal quantum numbers, where the series clearly converge to a particular fine-structure level of the $^2D^\circ$ state, J_cK (or jl) coupling is most appropriate.[23] In this coupling scheme, the spin and orbital angular momentum of the ion core are coupled to give the total angular momentum of the ion core, J_c. The orbital angular momentum of the Rydberg electron, l, is then coupled to J_c to give the resultant K. The spin of the Rydberg electron, s, is next coupled to K to give J, and the resulting states are labeled, for example, $(^2D^\circ_{J_c})nl[K]_J$. The coupling of s to K results in pairs of levels, and the splitting between them is generally quite small. Table I gives the $(^2D^\circ)ns'$ and nd' Rydberg series in J_cK coupling that are allowed in single-photon transitions from the $^1F_3$ level. The relative intensities of these series are discussed in more detail in Sec. V.

TABLE I. Rydberg states in J_cK coupling allowed in single-photon transitions from the $^1F_3$ level.

$(^2D^\circ_{5/2})ns'[K]_J$	$(^2D^\circ_{3/2})ns'[K]_J$	$(^2D^\circ_{5/2})nd'[K]_J$	$(^2D^\circ_{3/2})nd'[K]_J$
$(^2D^\circ_{5/2})ns'[\frac{5}{2}]_2$	$(^2D^\circ_{3/2})ns'[\frac{3}{2}]_2$	$(^2D^\circ_{5/2})nd'[\frac{3}{2}]_2$	$(^2D^\circ_{3/2})nd'[\frac{3}{2}]_2$
$(^2D^\circ_{5/2})ns'[\frac{5}{2}]_3$		$(^2D^\circ_{5/2})nd'[\frac{5}{2}]_2$	$(^2D^\circ_{3/2})nd'[\frac{5}{2}]_2$
		$(^2D^\circ_{5/2})nd'[\frac{5}{2}]_3$	$(^2D^\circ_{3/2})nd'[\frac{5}{2}]_3$
		$(^2D^\circ_{5/2})nd'[\frac{7}{2}]_3$	$(^2D^\circ_{3/2})nd'[\frac{7}{2}]_3$
		$(^2D^\circ_{5/2})nd'[\frac{7}{2}]_4$	$(^2D^\circ_{3/2})nd'[\frac{7}{2}]_4$
		$(^2D^\circ_{5/2})nd'[\frac{9}{2}]_4$	

IV. RESULTS AND DISCUSSION

A. Feasibility of double-resonance studies

The collection efficiency of the magnetic bottle electron spectrometer is ~50%, that is, ~1000 times higher than that of conventional electron spectrometers,[16] and it is this improvement in collection efficiency that allows us to record the wavelength dependence of the photoelectron spectra in the present study. However, while our earlier photoelectron spectra of atomic oxygen were recorded with a field-free ionization region, the magnetic bottle spectrometer requires a 1-T magnetic field.[16] Because the $^1F_3$ level is coupled to the $^4S^\circ_{3/2}$ continuum by the spin-spin interaction, it is possible that the external field could substantially decrease the lifetime of the $^1F_3$ level and make double-resonance studies via the $^1F_3$ level extremely difficult. Although the laser linewidth and Doppler broadening in the present experiments make it impossible to determine the lifetime of the $^1F_3$ level by a measurement of the linewidth of the $^1F_3 \leftarrow {}^1D_2$ two-photon transition, the lower frame of Fig. 2 shows the one-color photoelectron spectrum obtained with the magnetic bottle spectrometer with the laser tuned to the $^1F_3 \leftarrow {}^1D_2$ transition and with a pulse energy of ~20 μJ. The relative intensities of the $^4S^\circ_{3/2}$ photoelectron peak (corresponding to autoionization) and of the $^2D^\circ$ photoelectron peak (corresponding to photoionization from the $^1F_3$ level into the $^2D^\circ$ continuum) are comparable to those observed in the field-free photoelectron spectrum recorded previously.[9] This indicates that the $^1F_3$ lifetime is not significantly decreased by the 1-T field of the magnetic bottle spectrometer. Because the magnetic bottle spectrometer is essentially a modified time-of-flight spectrometer,[16] the energy resolution degrades with increasing electron kinetic energy, as is clearly visible in the lower frame of Fig. 2.

The upper frame of Fig. 2 shows the photoelectron spectrum obtained by tuning the pump laser to the $^1F_3 \leftarrow {}^1D_2$ two-photon transition and introducing the 354.7-nm third harmonic from the Nd:YAG laser as the probe beam. The new photoelectron peak at 0.686 eV corresponds to photoionization from the $^1F_3$ level into the $^2D^\circ$ continuum by the 354.7-nm beam. This clearly demonstrates that double-resonance experiments via the $^1F_3$ level are feasible. When the probe beam is present, not only does the new photoelectron peak appear, but the intensities of the two pump-only peaks (particularly the $^4S^\circ_{3/2}$ peak) also decrease. Depending on the alignment and intensity of the probe laser beam, the pump-only $^4S^\circ_{3/2}$ peak was observed to decrease in intensity by as much as 80%.

B. $^2D^\circ_{5/2}$ and $^2D^\circ_{3/2}$ ionization thresholds

Figure 3 shows the two-color photoionization spectrum of atomic oxygen that was obtained by pumping the two-photon $^1F_3 \leftarrow {}^1D_2$ transition and scanning the probe laser across the $^2D^\circ + e^- \leftarrow {}^1F_3$ photoionization threshold. The spectrum was obtained by setting the gate of the analog-to-digital converter to accept only those photoelectrons with near-zero kinetic energy (0–20 meV), as these will be produced just above the $^2D^\circ$ threshold. With the laser wavelengths and intensities used, no other

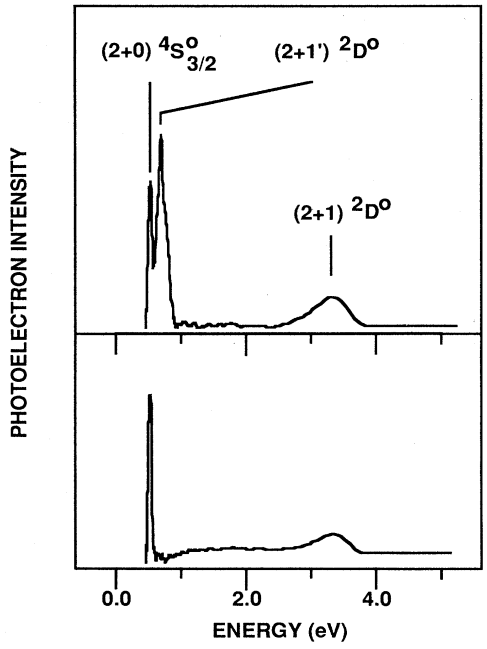

FIG. 2. The lower frame shows the one-color photoelectron spectrum of atomic oxygen with the laser tuned to the two-photon $(^2D^\circ)3p\ ^1F_3 \leftarrow {}^1D_2$ transition. The upper frame shows the same spectrum when the 354.7-nm beam from the Nd:YAG laser is introduced simultaneously with the pump beam.

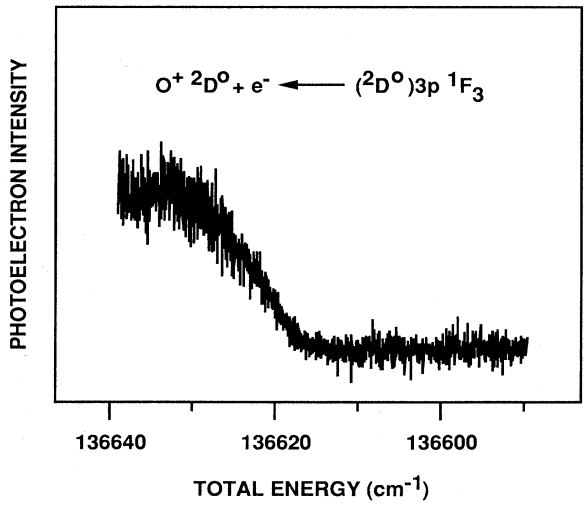

FIG. 3. Two-color spectrum of atomic oxygen obtained by monitoring the low-energy (0.00–0.02 eV) photoelectron signal. The pump laser was tuned to the $(^2D^\circ)3p\ ^1F_3 \leftarrow {}^1D_2$ transition, and the probe laser was scanned through the $O^+ {}^2D^\circ + e^- \leftarrow {}^1F_3$ ionization threshold.

photoionization process in atomic oxygen will produce photoelectrons within this range of kinetic energies. However, to obtain a reasonable collection efficiency of the slow electrons it was necessary to apply a small dc electric field (10 V/cm) across the ionization region of the electron spectrometer.

The photoionization spectrum in Fig. 3 displays a sharp onset that rises above the background level at 136 617 cm^{-1} total energy and reaches at plateau at $\sim$136 628 cm^{-1}. This onset is somewhat below the energetic threshold for the $O^+ {}^2D^\circ_{5/2}$ ionic state (136 647.67 cm^{-1}).[10,21,22] This shift is due primarily to electric field ionization of high Rydberg states converging to the $^2D^\circ_{5/2}$ threshold. Field ionization of Rydberg states with principal quantum number n by the external dc electric field is important for field strengths $F=5.142\times10^9/(16n^4)$, with F in V/cm.[24] For 10 V/cm, this will produce a shift in the ionization threshold of $\sim$19 cm^{-1}, in fair agreement with the observed shift.

Although a magnetic field cannot produce ionization in a stationary atom, an atom moving in a magnetic field does experience an equivalent electric field of magnitude $F_B=10^8 v_\perp B$, where $v_\perp$ is the velocity perpendicular to the magnetic field in cm/sec, B is the magnetic field strength in G, and F_B is in V/cm.[25] Unfortunately, it is not possible to make a good estimate of the average velocity $v_\perp$ without a knowledge of the N_2O photofragmentation dynamics and, in particular, of the translational energy of the $O\,{}^1D_2$ photofragment.[13] A large distribution of fragment translational energies could be responsible for the width of the step at threshold (which is considerably larger than the resolution width) because oxygen atoms of different velocities will produce difference effective electric fields. Collisional ionization will also shift the observed ionization threshold from the true energetic threshold.[26–28] Unfortunately, the collisional ionization rate is also difficult to estimate without a knowledge of the average velocities of the oxygen atoms. However, the relatively low pressure in the ionization region of the electron spectrometer makes it likely that electric field ionization is more important than collisional ionization in explaining the shift of the $^2D^\circ_{5/2}$ threshold.

The energetic threshold for the $O^+ {}^2D^\circ_{3/2}$ ionization continuum is 136 667.46 cm^{-1},[10] and the observed onset for ionization into this continuum is expected to be shifted to lower energy for the same reasons that the $^2D^\circ_{5/2}$ onset is shifted. However, Fig. 3 shows that above the $^2D^\circ_{5/2}$ threshold, the ionization signal reaches a plateau, and that no second step occurs at the $^2D^\circ_{3/2}$ threshold. This is readily understood in terms of the continuity of oscillator strength and the finite bandwidth of the probe laser. The continuity of oscillator strength of a Rydberg series through the ionization threshold is well known.[29] Above the $^2D^\circ_{5/2}$ threshold, autoionization of the $(^2D^\circ_{3/2})ns'$ and nd' series excited from the $^1F_3$ level into the $^2D^\circ_{5/2}$ continuum is allowed and expected to be fast. In addition, because the $^2D^\circ_{5/2}$ threshold is only 19.79 cm^{-1} below the $^2D^\circ_{3/2}$ threshold, the density of Rydberg states is extremely high, and individual series members cannot be resolved with the existing laser bandwidth. Therefore the excitation and subsequent autoionization of the series converging to the $^2D^\circ_{3/2}$ threshold cannot be distinguished from the $^2D^\circ_{5/2}$ direct ionization continuum or from direct ionization above the $^2D^\circ_{3/2}$ threshold. Thus no step is observed at the $^2D^\circ_{3/2}$ threshold. The best measure of the relative oscillator strengths of the $^2D^\circ_{5/2}$ and $^2D^\circ_{3/2}$ continuum therefore comes from the relative intensities of the Rydberg series converging to the two limits. A second approach is to use a zero-electron-kinetic-energy photoelectron spectrometer[30] with resolution much higher than the 21.0-cm^{-1} $^2D^\circ_{5/2}$-$^2D^\circ_{3/2}$ splitting. This approach would provide a direct measurement of the relative strengths of the two continua at threshold.

C. Rydberg series converging to the $^2D^\circ_{5/2}$ and $^2D^\circ_{3/2}$ limits

On the basis of the continuity of oscillator strength through an ionization threshold,[29] the large step at the $^2D^\circ_{5/2}$ ionization threshold implies that high Rydberg states converging to the $^2D^\circ_{5/2}$ and $^2D^\circ_{3/2}$ thresholds must also be populated with good probability. If these Rydberg states decay by autoionization into the $^4S^\circ_{3/2}$ continuum, they will produce fast photoelectrons with $\sim$3.3 eV of kinetic energy. Thus, by scanning the probe laser in the region below the $^2D^\circ_{5/2}$ ionization threshold and by monitoring the fast photoelectrons produced by autoionization, it should be possible to record the spectrum from the $^1F_3$ level to the Rydberg series converging to the $^2D^\circ_{5/2}$ and $^2D^\circ_{3/2}$ ionization limits. It should also be possible to record this spectrum by monitoring the decrease in the pump-only photoelectron peak at 0.516 eV as the probe laser is scanned; this technique would have the advantage of being independent of the decay pathway of the upper levels of the transitions. Although both techniques work, the former technique was used to record all of the spectra discussed below. It should be noted that the fast photoelectrons resulting from the two-color process appear at nearly the same electron kinetic energy as those from the one-color, three-photon process that produces $O^+ {}^2D^\circ$. Thus this one-color process produces a small constant background signal in the two-color spectrum. In the discussion that follows, the spectroscopic results and analysis will be presented first, followed by a discussion of the autoionization mechanism.

Figure 4 shows a portion of the double-resonance spectrum obtained by pumping the two-photon $^1F_3 \leftarrow {}^1D_2$ transition and probing in the region of total energy between 136 200 and 136 640 cm^{-1}. The portion of the spectrum in Fig. 4 displays a number of sharp transitions, and the structure throughout the region from 136 200 to 136 640 cm^{-1} is similar and quite regular. The energy levels, assignments, effective principal quantum numbers, and quantum defects for the upper levels of these transitions are given in Tables II–V. The sloped background level in Fig. 4 is due to a slow decrease in the pump laser power (and thus in the three-photon, pump-only photoelectron signal discussed above) as the probe laser was scanned from high to low energy.

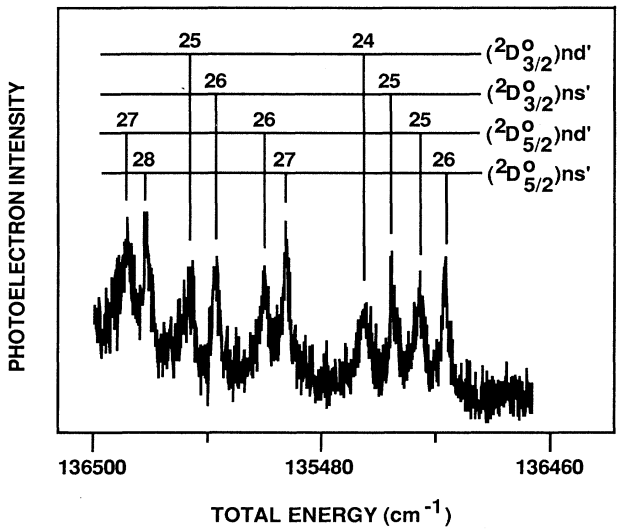

FIG. 4. Two-color spectrum of atomic oxygen obtained by monitoring the fast (3.3 eV) photoelectron signal. The pump laser was tuned to the two-photon $(^2D^\circ)3p\ ^1F_3 \leftarrow ^1D_2$ transition, and the probe laser was scanned through the region of interest.

The assignment of the observed transitions was made on the basis of quantum defects and on the earlier photoabsorption work of Huffman, Larrabee, and Tanaka.[21,22] The effective principal quantum number for each level was calculated with respect to both the $^2D^\circ_{5/2}$ and $^2D^\circ_{3/2}$ ionization limits by using the relation

TABLE II. $(^2D^\circ_{5/2})ns'[\frac{5}{2}]_2$ Rydberg states excited from the $(^2D^\circ)3p\ ^1F_3$ level.

Designation	Energy[a]	n^* [b]	μ [c]
$(^2D^\circ_{5/2})18s'[\frac{5}{2}]_2$	136 259.4	16.811	1.189
$(^2D^\circ_{5/2})19s'[\frac{5}{2}]_2$	136 301.9	17.815	1.185
$(^2D^\circ_{5/2})20s'[\frac{5}{2}]_2$	136 337.5	18.809	1.191
$(^2D^\circ_{5/2})21s'[\frac{5}{2}]_2$	136 368.1	19.81	1.19
$(^2D^\circ_{5/2})22s'[\frac{5}{2}]_2$	136 394.3	20.81	1.19
$(^2D^\circ_{5/2})23s'[\frac{5}{2}]_2$	136 417.0[d]	21.81	1.19
$(^2D^\circ_{5/2})24s'[\frac{5}{2}]_2$	136 437.1	22.83	1.17
$(^2D^\circ_{5/2})25s'[\frac{5}{2}]_2$	136 454.2	23.82	1.18
$(^2D^\circ_{5/2})26s'[\frac{5}{2}]_2$	136 469.4	24.81	1.19
$(^2D^\circ_{5/2})27s'[\frac{5}{2}]_2$	136 483.1	25.82	1.18
$(^2D^\circ_{5/2})28s'[\frac{5}{2}]_2$	136 495.4	26.84	1.16
$(^2D^\circ_{5/2})29s'[\frac{5}{2}]_2$	136 506.1	27.84	1.16
$(^2D^\circ_{5/2})30s'[\frac{5}{2}]_2$	136 515.8	28.85	1.15
$(^2D^\circ_{5/2})31s'[\frac{5}{2}]_2$	136 524.5	29.85	1.15

[a]All energies are with respect to the $O\ ^3P_2$ ground state are calculated by using the $^1F_3$ term energy of 113 996.239 cm^{-1} from Ref. 12.
[b]The n^* values were calculated from the relation $n^*=[R_O/(E_{IP}-E)]^{1/2}$, where R_O is the Rydberg constant for atomic oxygen (109 733.55 cm^{-1} from Ref. 31), E_{IP} is the $^2D^\circ_{5/2}$ ionization threshold (136 647.67 cm^{-1} from Ref. 10), and E is the energy of the Rydberg level.
[c]The quantum defect $\mu=n-n^*$.
[d]Blended with the $(^2D^\circ_{3/2})21d'$ transition.

TABLE III. $(^2D^\circ_{3/2})ns'[\frac{3}{2}]_2$ Rydberg states excited from the $(^2D^\circ)3p\ ^1F_3$ level.

Designation	Energy[a]	n^* [b]	μ [c]
$(^2D^\circ_{3/2})17s'[\frac{3}{2}]_2$	136 228.1	15.805	1.195
$(^2D^\circ_{3/2})18s'[\frac{3}{2}]_2$	136 278.9	16.805	1.195
$(^2D^\circ_{3/2})19s'[\frac{3}{2}]_2$	136 321.4	17.807	1.193
$(^2D^\circ_{3/2})20s'[\frac{3}{2}]_2$	136 357.2	18.806	1.194
$(^2D^\circ_{3/2})21s'[\frac{3}{2}]_2$	136 387.6	19.80	1.20
$(^2D^\circ_{3/2})22s'[\frac{3}{2}]_2$	136 413.9	20.80	1.20
$(^2D^\circ_{3/2})23s'[\frac{3}{2}]_2$	136 437.1	21.83	1.17
$(^2D^\circ_{3/2})24s'[\frac{3}{2}]_2$	136 456.6[d]	22.81	1.19
$(^2D^\circ_{3/2})25s'[\frac{3}{2}]_2$	136 473.8	23.80	1.20
$(^2D^\circ_{3/2})26s'[\frac{3}{2}]_2$	136 489.3	24.82	1.18
$(^2D^\circ_{3/2})27s'[\frac{3}{2}]_2$	136 502.9	25.82	1.18
$(^2D^\circ_{3/2})28s'[\frac{3}{2}]_2$	136 514.8	26.81	1.19
$(^2D^\circ_{3/2})29s'[\frac{3}{2}]_2$	136 525.5[e]	27.80	1.20

[a]All energies are with respect to the $O\ ^3P_2$ ground state and are calculated by using the $^1F_3$ term energy of 113 996.239 cm^{-1} from Ref. 12.
[b]The n^* values were calculated from the relation $n^*=[R_O/(E_{IP}-E)]^{1/2}$, where R_O is the Rydberg constant for atomic oxygen (109 733.55 cm^{-1} from Ref. 31), E_{IP} is the $^2D^\circ_{3/2}$ ionization threshold (136 667.46 cm^{-1} from Ref. 10), and E is the energy of the Rydberg level.
[c]The quantum defect $\mu=n-n^*$.
[d]Blended with the $(^2D^\circ_{5/2})24d'$ transition.
[e]Blended with the $(^2D^\circ_{5/2})30d'$ transition.

TABLE IV. $(^2D^\circ_{5/2})nd'$ Rydberg states excited from the $(^2D^\circ)3p\ ^1F_3$ level.

Designation	Energy[a]	n^* [b]	μ [c]
$(^2D^\circ_{5/2})16d'$	136 214.7	15.920	0.080
$(^2D^\circ_{5/2})17d'$	136 266.6	16.969	0.031
$(^2D^\circ_{5/2})18d'$	136 307.8	17.969	0.031
$(^2D^\circ_{5/2})19d'$	136 342.5	18.96	0.04
$(^2D^\circ_{5/2})20d'$	136 372.3	19.96	0.04
$(^2D^\circ_{5/2})21d'$	136 398.0	20.96	0.04
$(^2D^\circ_{5/2})22d'$	136 420.2	21.96	0.04
$(^2D^\circ_{5/2})23d'$	136 439.7	22.97	0.03
$(^2D^\circ_{5/2})24d'$	136 456.6[d]	23.96	0.04
$(^2D^\circ_{5/2})25d'$	136 471.4	24.95	0.05
$(^2D^\circ_{5/2})26d'$	136 484.9	25.96	0.04
$(^2D^\circ_{5/2})27d'$	136 496.8	26.97	0.03
$(^2D^\circ_{5/2})28d'$	136 507.6	27.99	0.01
$(^2D^\circ_{5/2})29d'$	136 517.0	28.98	0.02
$(^2D^\circ_{5/2})30d'$	136 525.5[e]	29.97	0.03

[a]All energies are with respect to the $O\ ^3P_2$ ground state and are calculated by using the $^1F_3$ term energy of 113 996.239 cm^{-1} from Ref. 12.
[b]The n^* values were calculated from the relation $n^*=[R_O/(E_{IP}-E)]^{1/2}$, where R_O is the Rydberg constant for atomic oxygen (109 733.55 cm^{-1} from Ref. 31), E_{IP} is the $^2D^\circ_{5/2}$ ionization threshold (136 647.67 cm^{-1} from Ref. 10), and E is the energy of the Rydberg level.
[c]The quantum defect $\mu=n-n^*$.
[d]Blended with the $(^2D^\circ_{3/2})24s'[\frac{3}{2}]_2$ transition.
[e]Blended with the $(^2D^\circ_{3/2})29s'[\frac{3}{2}]_2$ transition.

TABLE V. $(^2D^\circ_{3/2})nd'$ Rydberg states excited from the $(^2D^\circ)3p\ ^1F_3$ level.

Designation	Energy[a]	n^* [b]	μ [c]
$(^2D^\circ_{3/2})16d'$	136 236.8	15.963	0.037
$(^2D^\circ_{3/2})17d'$	136 286.1	16.963	0.037
$(^2D^\circ_{3/2})18d'$	136 327.2	17.958	0.042
$(^2D^\circ_{3/2})19d'$	136 362.3	18.963	0.037
$(^2D^\circ_{3/2})20d'$	136 391.9	19.96	0.04
$(^2D^\circ_{3/2})21d'$	136 417.0[d]	20.93	0.07
$(^2D^\circ_{3/2})22d'$	136 439.7	21.95	0.05
$(^2D^\circ_{3/2})23d'$	136 459.3	22.96	0.04
$(^2D^\circ_{3/2})24d'$	136 476.3	23.96	0.04
$(^2D^\circ_{3/2})25d'$	136 491.5	24.97	0.03
$(^2D^\circ_{3/2})26d'$	136 504.7	25.97	0.03
$(^2D^\circ_{3/2})27d'$	136 515.8	26.90	0.10

[a]All energies are with respect to the O $^3P_2$ ground state and are calculated by using the $^1F_3$ term energy of 113 996.239 cm^{-1} from Ref. 12.

[b]The n^* values were calculated from the relation $n^*=[R_O/(E_{IP}-E)]^{1/2}$, where R_O is the Rydberg constant for atomic oxygen (109 733.55 cm^{-1} from Ref. 31), E_{IP} is the $^2D^\circ_{3/2}$ ionization threshold (136 667.46 cm^{-1} from Ref. 10), and E is the energy of the Rydberg level.

[c]The quantum defect $\mu=n-n^*$.

[d]Blended with the $(^2D^\circ_{5/2})23s'[\frac{5}{2}]_2$ transition.

$n^*=[R_O/E_{IP}-E)]^{1/2}$, where R_O is the Rydberg constant for atomic oxygen (109 733.55 cm^{-1}),[31] E_{IP} is the $^2D^\circ_{5/2}$ or $^2D^\circ_{3/2}$ ionization threshold (136 647.67 and 136 667.46 cm^{-1}, respectively),[10] and E is the energy of the observed level. From the quantum defects ($\mu=n-n^*$) and the resulting Lu-Fano plot,[32] it is clear that the series do not interact very strongly. It is also clear that two of the series converge to the $^2D^\circ_{5/2}$ ionization limit while the other two converge to the $^2D^\circ_{3/2}$ limit. The appropriate values of n^* and μ are given in Tables II–V.

None of the levels observed in the present experiment has been observed previously. However, lower members of some $(^2D^\circ_{5/2,3/2})ns'$ and nd' series have been observed previously in photoabsorption studies from the ^3P, $^1D_2$, and $^1S_0$ levels by Huffman, Larrabee, and Tanaka[21,22] and in photoionization studies from the ^3P levels by Dehmer *et al.*[33–35] The $(^2D^\circ_{5/2,3/2})ns'$ series have quantum defects of 1.1 to 1.2 (0.1–0.2 if the values are given mod 1), and the $(^2D^\circ_{5/2,3/2})nd'$ series have quantum defects of 0.03 to −0.04. Thus the series in Tables II and III are clearly ns' series, and the series in Tables IV and V are clearly nd' series. We discuss the ns' series first.

In LS coupling, the $(^2D^\circ)ns'$ configuration gives rise to $^3D^\circ_{1,2,3}$ and $^1D^\circ_2$ levels; because of the $\Delta J=0,\pm1$ selection rule, the $J=1$ level cannot be observed in transitions from the $^1F_3$ level. Huffman, Larrabee, and Tanaka observed transitions to the $n=5-13$ members of the $^3D^\circ_{2,3}$ series from the $1s^22s^22p^4\ ^3P$ ground state[22] and transitions to the $^1D^\circ_2$ Rydberg series from the $1s^22s^22p^4\ ^1D_2$ level.[21] Within LS coupling, only transitions to higher-energy singlet levels are expected from the $^1F_3$ level. Thus, while transitions to the $(^2D^\circ)ns'\ ^1D^\circ_2$ levels are expected, transitions to the $(^2D^\circ)ns'\ ^3D^\circ_2$ and $^3D^\circ_3$ levels are forbidden. However, at higher principal quantum numbers, the approximations of LS coupling are no longer valid. Initially this breakdown is caused by the interaction of levels with the same configuration and total angular momentum, i.e., by the interaction of the $(^2D^\circ)ns'\ ^3D^\circ_2$ and $^1D^\circ_2$ levels.

The principal quantum number at which LS coupling breaks down can be estimated by comparing the $^3D^\circ_2$-$^1D^\circ_2$ energy difference for a given value of n and from the $^2D^\circ_{5/2}$-$^2D^\circ_{3/2}$ energy difference. The splitting between the $^3D^\circ_2$ and $^1D^\circ_2$ levels is caused by electron correlation effects. At low n, this splitting is much larger than the spin-orbit splitting between the $O^+\ ^2D^\circ_{5/2}$ and $^2D^\circ_{3/2}$ levels.[31] This means that correlation effects must be considered first, with the spin-orbit interaction considered subsequently as a perturbation, in what is essentially the regime of LS coupling. Because electron correlation effects, and thus the $^3D^\circ_2$-$^1D^\circ_2$ splitting, are expected to scale as $1/n^{*3}$, at very high n the $^2D^\circ_{5/2}$-$^2D^\circ_{3/2}$ splitting will be much larger than the $^3D^\circ_2$-$^1D^\circ_2$ splitting. In this regime, the spin-orbit splitting of the ion core must be considered first, with the effects of electron correlation considered as a perturbation. This corresponds to the regime of jj or J_cK coupling, in which the Rydberg electron is coupled to a particular spin-orbit state of the $^2D^\circ$ ion core.[23,31,36]

The intermediate regime in which the transition from LS to J_cK coupling takes place will occur when the $^3D^\circ_2$-$^1D^\circ_2$ splitting is approximately equal to the $^2D^\circ_{5/2}$-$^2D^\circ_{3/2}$ splitting of 21.0 cm^{-1}.[36] The data of Huffman, Larrabee, and Tanaka[21,22] indicate that this occurs at approximately $n=9$; therefore one expects to see a breakdown in LS coupling at approximately this point in the series. The range of n values probed in the double-resonance experiments is much higher than this, and therefore $(^2D^\circ)ns'$, J_cK coupled states allowed in transitions from the $^1F_3$ level correspond to the $(^2D^\circ_{5/2})ns'[\frac{5}{2}]_2$, $(^2D^\circ_{5/2})ns'[\frac{5}{2}]_3$, and $(^2D^\circ_{3/2})ns'[\frac{3}{2}]_2$.

Although the high Rydberg levels are best described in J_cK coupling, the oscillator strength to the $(^2D^\circ)ns'$, J_cK levels from the $^1F_3$ level still derives from the amount of singlet character (in this case, of $^1D^\circ_2$ character) in the J_cK levels. Thus, in the single-configuration approximation, the $(^2D^\circ_{5/2})ns'[\frac{5}{2}]_3$ levels will have no oscillator strength because they can contain no $^1D^\circ_2$ (that is, $J=2$) character. This consideration implies that the series in Tables II and III can be unambiguously assigned as the $(^2D^\circ_{5/2})ns'[\frac{5}{2}]_2$ and $(^2D^\circ_{3/2})ns'[\frac{3}{2}]_2$ series, respectively. The transformation between LS and J_cK coupling shows that the $(^2D^\circ_{5/2})ns'[\frac{5}{2}]_2$ levels have 60% $^1D^\circ_2$ character and that the $(^2D^\circ_{3/2})ns'[\frac{3}{2}]_2$ levels have 40% $^1D^\circ_2$ character.[23] Thus the oscillator strengths of these two series should be comparable, as is observed in our spectra. It is also interesting to note that at lower energies Huffman, Larrabee, and Tanaka[21] have observed the nominally forbidden transitions from the $^1D_2$ level to the $(^2D^\circ)ns'\ ^3D^\circ_2$ levels for principal quantum numbers $n\geq8$, in very good agreement with our prediction of the principal quantum

number at which the LS coupling approximation breaks down.

The assignment of the $(^2D^\circ_{5/2,3/2})nd'$ Rydberg series is more ambiguous than that of the $(^2D^\circ_{5/2,3/2})ns'$ series. As in the case of the $(^2D^\circ)ns'$ levels, the $(^2D^\circ)nd'$ levels are well described by LS coupling at low principal quantum number ($\sim n \leq 9$). Huffman, Larrabee, and Tanaka have observed the $n=3-14$ members of the $(^2D^\circ)nd'$ $^1D^\circ_1$, $^1D^\circ_2$, and $^1F^\circ_3$ Rydberg series in transitions from the $^1D_2$ level[21] and the $n=3-16$ members of the $^3P^\circ_2$ and $^3D^\circ_{2,3}$ series in transitions from the ^3P ground state.[22] In LS coupling, the allowed transitions from the $^1F_3$ level are to the $^1D^\circ_2$, $^1F^\circ_3$, and $^1G^\circ_4$ Rydberg series. However, for $n \geq 9$ the $(^2D^\circ)nd$ levels are better described in J_cK coupling. The allowed series based on this configuration are given in Table I. The transformation[23] from J_cK coupling to LS coupling shows that all of the $(^2D^\circ)nd'$ J_cK coupled states in Table I contain at least some singlet character; that is, the $J=2$ states all have some $^1D^\circ_2$ character, the $J=3$ states have some $^1F^\circ_3$ character, and the $J=4$ states have some $^1G_4$ character. Thus, without a more detailed calculation of the transition probabilities it is not possible to assign the K and J values of the $(^2D^\circ_{5/2,3/2})nd'$ Rydberg series.

At the relatively high principal quantum numbers studied in this work, the observed $(^2D^\circ_{5/2,3/2})nd'$ Rydberg series could actually be the result of the blending of two or more series. For example, the data of Huffman, Larrabee, and Tanaka[21] show that the $(^2D^\circ_{3/2})6d'$ $^1D^\circ_2$ and $^1F^\circ_3$ levels are separated by only 4 cm^{-1}. Scaling this energy difference by $1/n^{*3}$ gives a separation of only 0.2 cm^{-1} at $n=16$, the lowest $(^2D^\circ)nd'$ level we have studied. This splitting is much smaller than the 0.8-cm^{-1} linewidth of the observed transition, indicating that blending of two or more series is indeed possible. The absolute assignment of the J and K values of the $(^2D^\circ_{5/2,3/2})nd'$ series will require the extension of the present results to lower principal quantum numbers, where the splitting between these levels will be observable.

D. Autoionization mechanism

Although it is clear from the spectrum shown in Fig. 4 that the $(^2D^\circ_{5/2,3/2})ns'$ and nd' Rydberg series autoionize into the $^4S^\circ_{3/2}$ ionization continuum, the autoionization mechanism has not yet been considered. Within LS coupling the singlet $(^2D^\circ)ns'$ and nd' Rydberg states are forbidden to autoionize and can only do so by spin-orbit and spin-spin interactions.[18,19] Because the autoionization rates are also expected to scale as $1/n^{*3}$, the rates for the high Rydberg states observed here should be very much smaller than those observed at low principal quantum numbers. However, the breakdown of LS coupling described above in the discussion of intensities is also important for an understanding of the autoionization rates. For example, at high n, the $(^2D^\circ_{5/2})ns'[\frac{5}{2}]_2$ and $(^2D^\circ_{3/2})ns'[\frac{3}{2}]_2$ levels have only 60% and 40% singlet character, respectively.[23] This observation implies that they also have 40% and 60% triplet character, respectively. This large amount of triplet character, which is not present in the Rydberg states at low n, can interact with the allowed triplet ionization continua based on the $O^+ {}^4S^\circ_{3/2}$ state and therefore can lead to rapid autoionization. In the range of principal quantum numbers studied in this paper, all of the observed series have substantial triplet character, and therefore autoionization into the $^4S^\circ_{3/2}$ continuum is allowed. Thus the breakdown of LS coupling can account for the "forbidden" autoionization observed in our experiment. Furthermore, the magnetic field employed in the magnetic bottle electron spectrometer may also increase the autoionization rates of the high Rydberg states through the linear Zeeman and diamagnetic interactions.[24]

For the lowest principal quantum numbers studied by Huffman, Larrabee, and Tanaka[21,22] (i.e., $n=3-6$), the approximations of LS coupling are expected to be quite good. Thus, for $n=3-6$, the singlet $(^2D^\circ)ns'$ and nd' Rydberg states excited from the $^1D_2$ level should have very small autoionization probabilities because autoionization of pure singlet states into the $^4S^\circ_{3/2}$ continuum is forbidden. What is striking is that in the O $^1D_2$ photoabsorption spectrum of Huffman, Larrabee, and Tanaka,[21] the singlet $(^2D^\circ)ns'$ and nd' levels with $n \leq 6$ or 7 are actually observed in *emission* rather than absorption. Although the kinetics of the processes involved in the discharge used to produce the O $^1D_2$ atoms are quite complicated, this observation can be explained if the $(^2D^\circ_{5/2,3/2})ns'$ and nd' Rydberg levels are also populated in the discharge. If the autoionization lifetime of these levels is long enough for emission to compete with autoionization and if the population in the Rydberg levels is high enough, emission from these levels will be stronger than absorption to these levels, and the spectrum will display emission lines. Because of the breakdown of LS coupling, however, for higher principal quantum numbers, the autoionization rate of the $(^2D^\circ_{5/2,3/2})ns'$ and nd' Rydberg states increases relative to the emission rate. This removal of population in the Rydberg levels by autoionization allows photoabsorption from the $^1D_2$ level to these levels to dominate over emission from them. Thus these levels will appear as absorption lines in the spectrum. In the intermediate regime, neither photoabsorption nor emission will dominate, and the observed transitions will be weak. This expectation is consistent with the observations of Huffman, Larrabee, and Tanaka.[21] Although a detailed understanding of the kinetics of the discharge is necessary to predict the value of n at which the transition from emission to absorption occurs, we have seen here that LS coupling breaks down at approximately $n=9$. In fact, Huffman, Larrabee, and Tanaka[21] observe the transition from emission to absorption at approximately $n=6$ or 7, in good agreement with our estimate.

E. Relation to high-intensity studies of ATI

The discussion of the double-resonance spectra in terms of transitions between long-lived autoionizing levels of atomic oxygen would have been exactly the same for transitions between bound states. However, because

both the lower and upper levels of the probe transitions in the spectra summarized in Tables II–V are embedded in the $^4S^\circ_{3/2}$ continuum, it is also possible to view the spectra as the wavelength dependence of the ATI signal. Mechanically, the escape of the electron is delayed in the quasibound Rydberg state, which absorbs another photon before it can decay. While transitions between autoionizing levels are certainly relevant to the discussion of ATI and direct multiphoton processes leading to multiple ionization,[1–5] no detailed experimental studies of these transitions have been performed. Figure 4 clearly shows that in certain instances transitions between autoionizing levels can produce sharp resonances in the ATI signal.

We have also examined the effect of the probe laser intensity on the spectrum of Fig. 4. An increase in the probe laser intensity by a factor of 10 causes saturation of the probe transition; that is, all of the resonance structure disappears, and the ATI signal is large and constant as a function of wavelength. This regime is likely to be applicable in almost all previous studies of ATI,[1–5] because at the high laser intensities required for the observation of nonresonant multiphoton ionization and ATI, single-photon transitions between autoionizing levels will nearly always be saturated. Thus only in more controlled experiments will the resonant structure of transitions between autoionizing states be revealed.

V. CONCLUSIONS

We have performed double-resonance studies of transitions between long-lived autoionizing states of atomic oxygen by pumping the two-photon $(^2D^\circ)3p\ ^1F_3 \leftarrow ^1D_2$ transition and probing transitions from the autoionizing $^1F_3$ level to higher-energy Rydberg levels. By using a magnetic bottle electron spectrometer to detect the ionization process of interest, we have observed for the first time the $(^2D^\circ_{5/2,3/2})ns'$ and $nd' \leftarrow ^1F_3$ transitions for $n = 16–30$. These spectra provide new information on the Rydberg series of atomic oxygen, especially with regard to the breakdown of LS coupling at high principal quantum numbers. We have also discussed the relationship between the present results and high-intensity studies of ATI.

The present results indicate that studies of the $(^2D^\circ)ns'$ and nd' series between $n=5$ and 9, that is, in the region of the transition from LS coupling to J_cK coupling, should be most interesting. In this region, the redistribution of oscillator strength occurs from the pure singlet states in LS coupling to the mixed-spin states in J_cK coupling, and, in addition, a dramatic change in the autoionization rates of the Rydberg states should occur. For this range of n, the spectrum obtained by monitoring the fast-photoelectron signal, which depends on the autoionization of the upper level, may show significant differences from the spectrum obtained by monitoring the decrease in the slow-electron signal, which requires only autoionization of the $^1F_3$ level into the $^4S^\circ_{3/2}$ continuum. These differences will provide much more detailed information on the breakdown of LS coupling in this region. If the upper level of the probe transition is very long lived, it may also be possible to photoionize the level into the $^2D^\circ$ continuum, thus producing a second ATI peak. Studies of this region of the spectrum are currently being planned.

ACKNOWLEDGMENTS

We would like to thank Dr. E. F. McCormack for her insight regarding several aspects of this work. This work was supported by the U.S. Department of Energy, Assistant Secretary for Energy Research, Office of Health and Environmental Research, under Contract No. W-31-109-ENG-38.

[1] A. L'Huillier, Comments At. Mol. Phys. **18**, 289 (1986).
[2] P. Lambropoulos, Comments At. Mol. Phys. **20**, 199 (1987).
[3] P. Agostini and G. Petite, Contemp. Phys. **29**, 57 (1988).
[4] See, for example, the special issue of J. Opt. Soc. Am. B **4**, 702 (1987).
[5] H. Bachau and P. Lambropoulos, Z. Phys. D **11**, 37 (1989).
[6] J. K. Spong, A. Imamoğlu, R. Buffa, and S. E. Harris, Phys. Rev. A **38**, 5617 (1988).
[7] L. D. Van Woerkom, J. G. Story, and W. E. Cooke, Phys. Rev. A **34**, 3457 (1986).
[8] T. F. Gallagher, R. Kachru, N. H. Tran, and H. B. van Linden van den Heuvell, Phys. Rev. Lett. **51**, 1753 (1983).
[9] S. T. Pratt, P. M. Dehmer, and J. L. Dehmer, Phys. Rev. A **43**, 282 (1991).
[10] C. E. Moore, *Atomic Energy Levels,* Natl. Bur. Stand. Ref. Data Ser., Natl. Bur. Stand. (U.S.) Circ. No. 35 (U.S. GPO, Washington, D.C., 1971), Vol. I; *Selected Tables of Atomic Spectra O I,* Natl. Stand. Ref. Data Ser., Natl. Bur. Stand. (U.S.) Circ. No. 3 (U.S. GPO, Washington, D.C., 1976), Sec. 7.
[11] B. Edlén, Kungl. Svenska. Vetenskapsakad. Handl. **20**, (10) (1943).
[12] K. B. S. Eriksson and H. B. S. Isberg, Ark. Fys. **37**, 221 (1968).
[13] H. Okabe, *Photochemistry of Small Molecules* (Wiley-Interscience, New York, 1978).
[14] S. Kröll, H. Lundberg, A. Persson, and S. Svanberg, Phys. Rev. Lett. **55**, 284 (1985).
[15] M. A. O'Halloran, S. T. Pratt, P. M. Dehmer, and J. L. Dehmer, J. Chem. Phys. **87**, 3288 (1987).
[16] P. Kruit and F. H. Read, J. Phys. E **16**, 313 (1983).
[17] B. A. Palmer, R. A. Keller, and R. Engleman, Jr., Los Alamos Scientific Laboratory, Internal Report No. LA-8251-MS, 1980 (unpublished).
[18] P. Feldman and R. Novick, Phys. Rev. **160**, 143 (1967).
[19] M. E. Rudd and K. Smith, Phys. Rev. **169**, 79 (1968).
[20] G. Herzberg, *Atomic Spectra and Atomic Structure* (Dover, New York, 1944).
[21] R. E. Huffman, J. C. Larrabee, and Y. Tanaka, J. Chem. Phys. **47**, 4462 (1967).
[22] R. E. Huffman, J. C. Larrabee, and Y. Tanaka, J. Chem. Phys. **46**, 2213 (1967).
[23] R. D. Cowan and K. L. Andrews, J. Opt. Soc. Am. **55**, 502 (1965).
[24] D. Kleppner, M. G. Littman, and M. L. Zimmerman, in *Ryd-*

berg States of Atoms and Molecules, edited by R. F. Stebbings and F. B. Dunning (Cambridge University Press, Cambridge, England 1983), p. 73.

[25]C. W. Clark, K. T. Lu, and A. F. Starace, in *Progress in Atomic Spectroscopy (Part C),* edited by H. J. Beyer and H. Kleinpoppen (Plenum, New York, 1984), p. 247.

[26]See, for example, M. Matsuzawa, in *Rydberg States of Atoms and Molecules* (Ref. 24), p. 267.

[27]F. B. Dunning and R. F. Stebbings, in *Rydberg States of Atoms and Molecules* (Ref. 24), p. 315.

[28]M. R. Flannery, in *Rydberg States of Atoms and Molecules* (Ref. 24), p. 393.

[29]U. Fano and J. W. Cooper, Rev. Mod. Phys. **40**, 441 (1968).

[30]K. Müller-Dethlefs, K. Sander, and E. W. Schlag, Chem. Phys. Lett. **112**, 291 (1984).

[31]B. W. Shore and D. H. Menzel, *Principles of Atomic Spectra* (Wiley, New York, 1968).

[32]K. T. Lu and U. Fano, Phys. Rev. A **2**, 81 (1970).

[33]P. M. Dehmer, J. Berkowitz, and W. A. Chupka, J. Chem. Phys. **59**, 5777 (1973).

[34]P. M. Dehmer and W. A. Chupka, J. Chem. Phys. **62**, 584 (1975).

[35]P. M. Dehmer, W. L. Luken, and W. A. Chupka, J. Chem. Phys. **67**, 195 (1977).

[36]I. I. Sobelman, *Atomic Spectra and Radiative Transitions* (Springer-Verlag, New York, 1970).